Magnetization of Pt_{13} clusters supported in a NaY zeolite: A XANES and XMCD study

J. Bartolomé,[1] F. Bartolomé,[1] L. M. García,[1] E. Roduner,[2] Y. Akdogan,[2] F. Wilhelm,[3] and A. Rogalev[3]
[1]*Instituto de Ciencia de Materiales de Aragón and Departamento de Física de la Materia Condensada, CSIC–Universidad de Zaragoza, 50009 Zaragoza, Spain*
[2]*Institut für Physikalische Chemie, Universität Stuttgart, Pfaffenwaldring 55, D-70569 Stuttgart, Germany*
[3]*European Synchrotron Radiation Facility, BP 220, F-38043 Grenoble, France*
(Received 9 February 2009; revised manuscript received 1 June 2009; published 2 July 2009)

X-ray absorption and x-ray magnetic circular dichroism (XMCD) spectra have been recorded at the Pt $L_{2,3}$ edges of Pt_{13} and hydrogenated $Pt_{13}H_m$ clusters dispersed in NaY zeolite. A Pt foil was also measured as reference for comparison with bulk Pt. From the x-ray absorption near edge structure measurements the average number of holes n_h in the $5d$ band of these systems is found. In the $Pt_{13}H_m$ sample the Pt-H antibonding state increases n_h with respect to the Pt_{13} sample. It gives rise to a shape resonance with energy $E_{res}=2.3$ eV. The average orbital and spin moments m_L and m_S for the Pt atom have been determined from the XMCD measurements. The total magnetic-moment field dependence XMCD(H) was determined and scaled to the absolute value of the average moment per Pt atom. The fit of XMCD(H) to a Langevin function yields a magnetic moment per cluster of $\mu=3.7\pm0.4$ and 3.0 ± 0.4 μ_B, for Pt_{13} and $Pt_{13}H_m$, respectively. It is shown that nonmagnetic clusters coexist with those giving magnetic signal. The amount of Pt constituting the magnetic Pt_{13} clusters is 15–20% of the total Pt content. The XMCD data are compared with superconducting quantum interference device magnetization measurements. The moment found indicates that the cluster spin of Pt_{13} and $Pt_{13}H_m$ is in the range $S\approx2-3$. They are compared to predictions calculated by density-functional methods.

DOI: 10.1103/PhysRevB.80.014404 PACS number(s): 36.40.Cg, 82.75.Vx, 78.70.Dm, 75.50.Tt

I. INTRODUCTION

The understanding of magnetism at the ultimate length scale is one of the current frontiers in solid-state physics. In particular, it is of paramount importance to disentangle how the bulk properties are modified in very small particles, where the atomic coordination is strongly reduced with respect to the bulk. This goal is in many cases complicated by two facts: first, an uncontrolled size distribution and second, the chemical bonds and magnetic interactions with the surroundings and between particles. Therefore, it is important to look for model systems in which properly finite-size phenomena can be studied.

Some metals whose bulk material do not fulfill the Stoner criterion to support spontaneous magnetic moment, such as Pt, may undergo a crossover to magnetic behavior by several ways: a neighboring magnetic material may polarize it, such as a Co thin film,[1,2] Co particles,[3] or when alloyed with transition metals such as Co,[4] or Fe.[5] The nonzero magnetic moment of Pt in all these cases has been determined unambiguously by means of x-ray magnetic circular dichroism (XMCD) at the Pt $L_{2,3}$ edges.

More interestingly, a perturbation of the Pt coordination or reduced dimensionality of the Pt system may cause the Pt to have a magnetic moment and create magnetic particles, as it takes place in Pt nanoparticles protected by poly-N-vinylpyrrolidine (PVP). With a diameter below 3 nm, Pt-PVP exhibits superparamagnetism and strongly enhanced magnetization ($\mu\approx5$ μ_B) compared to the paramagnetic moments in the bulk Pt.[6]

Zeolites are frequently used as support of Pt species in catalysis. For example, Pt in I and III valence states and Pt dimers which are known to yield to paramagnetic signals in electron paramagnetic resonance (EPR).[7] Recently, small Pt clusters supported in NaY zeolites, containing 13 ± 2 atoms have been reported.[8–10] These Pt particles are prepared in two chemical states: Pt_{13} particles covered by adsorbed H atoms in one case and Pt_{13} particles with H completely desorbed.[8] They are dispersed in a zeolite matrix with a Pt loading of 6% in weight. The cluster may sit on a puckered 6-ring window (SII site of the faujasite structure), in which three oxygen atoms point toward the cluster and three away from it. With this loading and Pt_{13} clusters dispersed randomly, one out of 25 supercages is occupied by a cluster. This corresponds to an average distance of 3.6 nm between clusters. From extended x-ray absorption fine structure (EXAFS) experiments[9,10] the structure of these clusters have been reported to be close to icosahedral, with a cluster size of 13 ± 2 Pt atoms and a diameter of 7 ± 1 Å, that is, a central Pt atom is surrounded by 12 atoms at the cluster surface (Fig. 1). The presence of other larger particles could be excluded. In absence of any external oxygen, a second near-neighbor shell contribution from the zeolite oxygen atoms could be detected.[10]

The first evidence that these clusters may have a magnetic moment was brought forward by the x-band EPR spectra of 6% Pt/NaY,[8] which showed a characteristic multiplet at $g=2.357$. The spectra could be simulated unambiguously assuming 12 equivalent Pt nuclei, implying that the source of the magnetic moment is at the 12 surface Pt atoms. Since most of the cluster molecular orbitals have a nodal plane through the center it is conceivable that there is very little spin population on the central atom, which leads to a small and unresolved hyperfine coupling. By calibrating the EPR signal and assuming that the observed species is spin-1/2 it was concluded that only on the order of 0.03% of the total Pt in the sample is EPR active.[8]

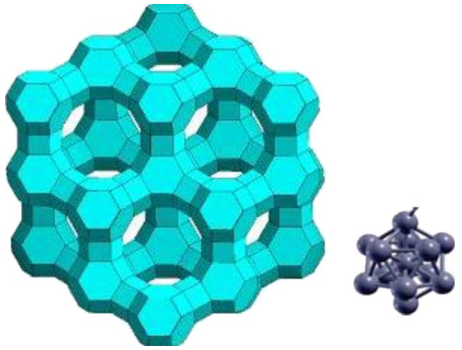

FIG. 1. (Color online) Left: NaY zeolite. Right: $Pt_{13}H_1^{+1}$ cluster (Ref. 8)

A more quantitative study of the particle magnetization was made using superconducting quantum interference device (SQUID) magnetometry.[9] The high-temperature susceptibility could be fitted assuming a paramagnetic Curie-type behavior and a superimposed temperature-independent contribution. No magnetic ordering anomaly was detected down to 1.8 K. The reported effective moment per Pt was $m_{Pt}=0.45(5)\ \mu_B$, assuming that all 13 Pt atoms were contributing. Such a value for a Pt cluster is the highest ever observed. The magnetization $M(H)$ curve at 1.8 K showed the characteristic shape of a Langevin-type paramagnet, with a reported moment $m_{Pt}=0.45$ and 0.43 μ_B per Pt, for Pt_{13} and $Pt_{13}H_m$, respectively.[9]

It was deemed that an XMCD study of this system could help in understanding the origin and value of the Pt_{13} cluster orbital and spin magnetic-moment components. Moreover, any magnetic contribution from magnetic impurities other than Pt in the zeolite could be ruled out because of the elemental selectivity of the XMCD technique. Since all but one Pt atom are at the surface, the surface effects attributable to the loss of local symmetry are maximized in this type of cluster, enabling us to ascribe the peculiar cluster physical properties to the surface atoms. In particular, the asymmetry of Pt coordination at the surface is expected to narrow the 5*d* electron "surface band," as it happens in 3*d* out-of-plane electron band of Co atoms at a Co/vacuum interface[11] or at a Co/Cu interface,[12] and produce a variation in the surface atomic-orbital moment, which may be discernible only with the XMCD technique.

The $Pt_{13}H_m$ clusters could, in principle, have a different magnetic moment than the bare one and some differences have been, indeed, reported.[8] However, just as for the Pt_{13}, the XMCD measurements may yield further evidence to the effect of cluster hydrogenation. Moreover, since the difference of the x-ray absorption spectroscopy (XAS) spectra at the $L_{2,3}$ edges of the bare and hydrogenated clusters gives relevant information on the Pt-H bonding, we have done a careful analysis of the x-ray absorption near edge structure (XANES) of these spectra.

II. EXPERIMENTAL

The Pt clusters were prepared in NaY zeolite by ion exchange with 3 mM aqueous $[Pt(NH_3)_4]Cl_2$ solution followed by stirring at 343 K for at least 48 h. The loading achieved is about 6 wt %. The sample was washed, dried, and calcined in flowing O_2 (20 mL min^{-1} g^{-1}) at a heating rate of 0.5 K min^{-1} from room temperature to 573 K and then holding that temperature for 5 h. Reduction was then performed in flowing hydrogen (25 mL min^{-1} g^{-1}) with a heating rate of 6 K min^{-1} to 473 K and keeping it at 473 K for 1 h. The hydrogen desorption was achieved by evacuating with a turbomolecular pump a glass tube containing the Pt/NaY powder while heating it in an oven at 418 K for 120 min. Two samples were prepared for this experiment, a hydrogen reduced, $Pt_{13}H_m$ and a fully desorbed one, Pt_{13}.

To prepare the sample for the XAS and XMCD experiment the sample was compressed in a pellet, protected at preparation in Ar. The pellet was inserted, in a glove box under Ar, in a custom-built sample holder, covered with a Kapton foil (0.2 mm thick), and sealed with a pressure ring. This capsule was screwed at the end of a temperature-controlled cold finger that was inserted in a superconducting cryomagnet.

The XAS and XMCD experiments were performed at the European Synchrotron Radiation Facility in Grenoble at the ID12 (Pt $L_{2,3}$ edges) beamline. The undulator APPLE-II was employed and a double-Si(111)-crystal monochromator provided a monochromatized beam. The polarization was over 95% in all cases. The detection technique used in the ID12 experiments was total fluorescence yield in backscattering geometry. The XMCD signal was obtained by a direct difference of the XAS spectra recorded with opposite helicities at each magnetic fixed field value, for both orientations of the field. The field was applied along the normal incidence to the sample plate.

The field-dependent measurements were performed at constant energy (at the energy of the XMCD L_3 peak) by changing the helicity of the incoming beam, at constant field for each point, and varying the field from +6 to −6 T and vice versa. In all measurements the temperature was kept constant at $T=7$ K.

The reference Pt film of 100 μm was also measured with the same instrument at $T=10$ K and an applied field of 7 T, with total fluorescence yield detection.

III. XAS RESULTS

The XAS spectra were obtained at the L_3 and L_2 edges of Pt on the Pt_{13} and $Pt_{13}H_m$ samples [Figs. 2(a), 3(a), and 4(a)]. In Fig. 5 the XAS at the L_3 edge of the Pt_{13} cluster is depicted together with the Pt-foil spectrum. In the XANES region a difference in the white line is observed and in the EXAFS region the undulation maxima also differ in energy and amplitude. The difference may be explained as due to their different Pt-Pt distances and number of neighbors. They are in reasonable agreement with the XAS spectrum calculated for a Pt_{13} cluster of cuboctahedral symmetry (Fig. 4).[13] Those authors performed density-functional theory (DFT) calculations which allow to model reconstructions of the Pt cluster. The geometry optimization procedure yielded for Pt_{13} an average bond length of 2.652 Å, in excellent agreement with the distance found from EXAFS experiments,[9]

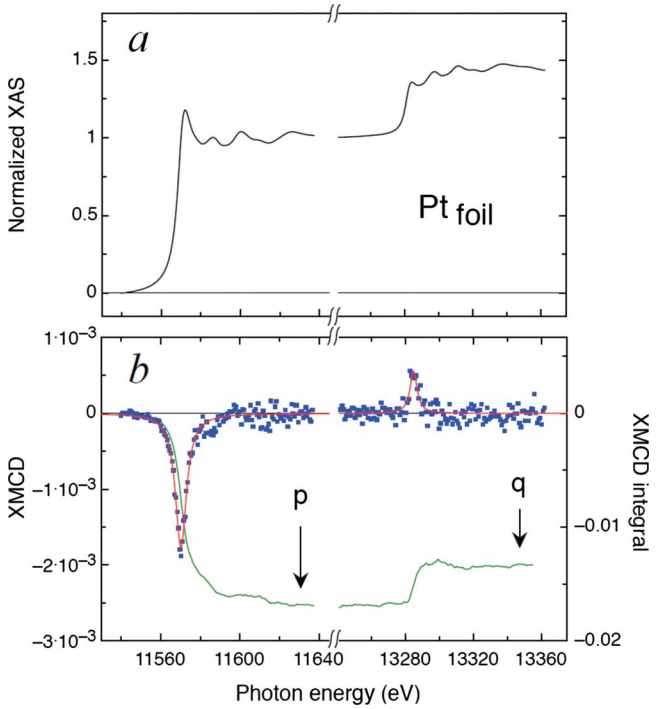

FIG. 2. (Color online) (a) Normalized isotropic Pt $L_{2,3}$-edges XAS spectra of the Pt-foil sample. (b) XMCD spectra. (●) Experimental points; (—) Fit to Lorentzian functions as guide to the eyes; (—) Area integral. The arrows indicate the higher limit of the p and q integrals.

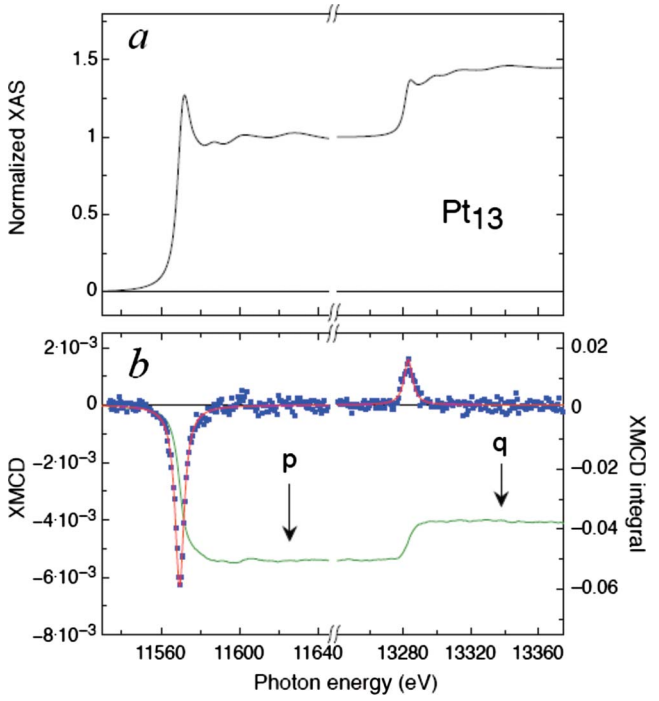

FIG. 3. (Color online) (a) Normalized isotropic Pt $L_{2,3}$-edges XAS spectra of the Pt_{13} sample. (b) XMCD spectra. (●) Experimental points; (—)Fit to Lorentzian functions as guide to the eyes; (—) Area integral. The arrows indicate the higher limit of the p and q integrals.

confirming the contraction of average Pt-Pt distance and the suitability of the proposed Pt_{13} regular model.

The average number of nearest neighbors, $N=5.54$, is practically identical to the value found in EXAFS measurements analyzed based on a single-Pt shell.[9] This result is of importance to prove that our Pt_{13} sample consists of a collection of clusters with the same geometry.

To establish a common reference E_0 for the Fermi energy for both L_2 and L_3 edges in the bare Pt_{13} cluster spectra the energy of maximum slope was chosen.[14] The L_2 edge of the $Pt_{13}H_m$ spectra was aligned with respect to the bare Pt_{13} L_2 edge at 0.6 of the step height. Finally, the L_3 edge was shifted as to match the oscillation at $E-E_0=58$ eV common to all samples. The obtained spectra are shown together with the spectra for a Pt foil, for sake of comparison [Fig. 6]. The differences in the XANES region are depicted in Figs. 6(a) and 6(b). Lower curves and the area differences have been evaluated. It is found that the XAS white line of the Pt_{13} desorbed is higher than that of Pt metal and the $Pt_{13}H_m$ is, in turn, slightly higher than the desorbed one, therefore, it can be qualitatively concluded, at first instance, that the hydrogenation has created some new holes, n_h, in the Pt $5d$ band. This in qualitative agreement with the conclusion reached in Ref. 10 that the n_h increases with respect to the reference Pt in $P_{13}H_m$ clusters.

The XAS spectra have been normalized taking into account the correction resulting from the fact that the ratio of the L_3 to L_2 edge jump deviates from the statistical ratio (i.e., $R=2$ the ratio corresponding to the degeneracy of the core-hole states). The ratio has been found experimentally for

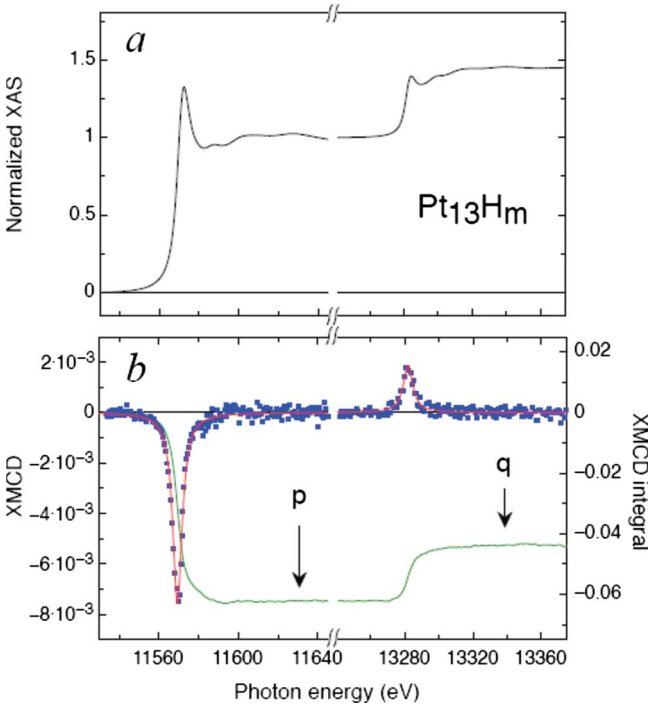

FIG. 4. (Color online) (a) Normalized isotropic Pt $L_{2,3}$-edges XAS spectra of the $Pt_{13}H_m$ sample. (b) XMCD spectra. (●) Experimental points; (—) Fit to Lorentzian functions as guide to the eyes; (—) Area integral. The arrows indicate the higher limit of the p and q integrals.

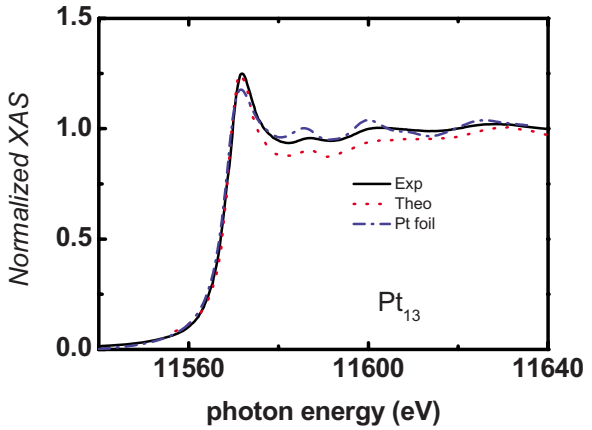

FIG. 5. (Color online) Comparison of the (-) XAS of Pt_{13} at the Pt L_3-edge, (- - -) calculated spectra for a Pt_{13} cuboctahedron, (Ref. 13) and for a Pt foil (-··-).

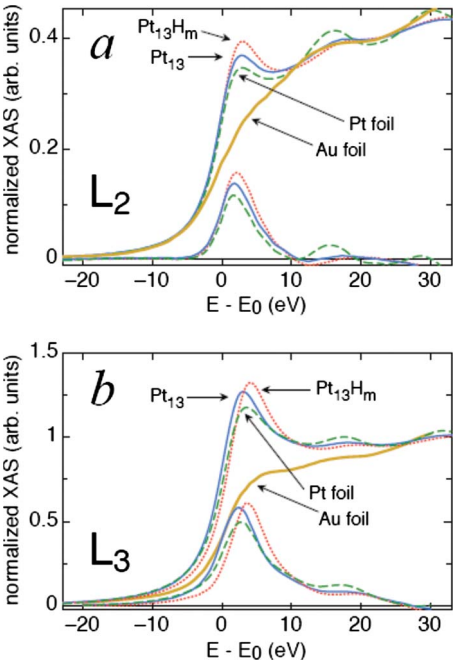

FIG. 6. (Color online) Comparison of the Pt XAS spectra. (a) At the L_2 edge, in photon energy relative to the E_0. (b) At the L_3 edge. (- -) Metal Pt foil, (—) Pt_{13}, (···) $Pt_{13}H_m$, (—) Au film. (Lower curves) White-line differences of the XAS curves with respect to the Au metal foil.

pure Pt to be $R=2.22$ (Ref. 15). In Figs. 6(a) and 6(b) the $L_{2,3}$ spectra of Pt_{13} and $Pt_{13}H_m$ are shown once that the EXAFS matching and normalization procedure has been done for metallic Pt and Au films.[12] In what follows, this normalization criterion has an effect in the determination of n_h and in the analysis of the XMCD spectra.

To obtain a quantitative determination of the average number of holes, n_h, the area differences, $r=I_{L2}+I_{L3}$ (where I_{L2} and I_{L3} are the white line integrated intensities after subtraction of the contributions from transitions to the continuum) need to be calculated. Since the white line is small, instead of subtracting a step function (or arc-tangent curve) the Au XAS white line is taken as reference, following closely the method proposed in Ref. 16. Indeed, in Au the $5d$ band is nearly full, and, therefore, the difference with respect to the Pt is large, therefore, a good evaluation of r may be done. The area differences for the three Pt spectra have been integrated between $E-E_0=-15$ and 25.5 eV, where E_0 is the energy at the inflection point of the XAS peak low-energy tail and are included in Table I.

Absolute values of n_h were calculated following the methodology described in Ref. 17. First, the difference between the Pt metal n_h^{Pt} and the Au metal n_h^{Au}, $\tilde{n}_h=n_h^{\mathrm{Pt}}-n_h^{\mathrm{Au}}=0.98$ ($n_h^{\mathrm{Pt}}=1.73$ and $n_h^{\mathrm{Au}}=0.75$) is calculated. Second, the scaling factor $C^{-1}=\tilde{n}_h/r_{\mathrm{Pt,film}}=0.132$ holes/eV is determined from the experiment for the Pt film, $r_{\mathrm{Pt,film}}=7.44$ eV. Third, the absolute number of holes for each Pt_{13} sample can be calculated as $n_h=n_h^{\mathrm{Au}}+C^{-1}r$. The results are included in Table I. The conclusion is that the number of holes per Pt atom, averaged to all Pt atoms in the sample, n_h, increases in the Pt_{13} samples with respect to the Pt film (bulk), and that hydrogenation also has the effect of increasing a small, but well detectable, number of holes in $Pt_{13}H_m$ with respect to the Pt_{13} desorbed one.

Since the enlightening paper of Hammer and Nørskov,[18] the important role of the energy and degree of filling in the Pt-H bonding and antibonding states in the reactivity of Pt, was recognized. The bonding state is well located in the H atom while in Pt it has been calculated that the antibonding state lies just above the Fermi energy, thus it creates empty states which may be determined from the difference between the XAS spectra of the Pt_n and the Pt_nH_m adsorbed cluster.[14] In Fig. 7 the XAS of the Pt $L_{2,3}$ edges are shown scaled to a common normalization so that the differences induced by the cluster electronic and geometrical variations are made more visible. In the inset a magnified picture near the XANES region shows clearly the difference induced by hydrogen uptake.

TABLE I. Parameters determined from XANES and XMCD experiments. H_{appl}, magnetic field applied in the experiment. r, area integral of the white line. n_h number of holes, p and q area integrals subtended by the L_3 and $L_{3,2}$ edges, respectively. Average m_L, m_S, and the ratio m_L/m_S calculated with the sum rules. m_{at}, average total magnetic moment ($m_{\mathrm{at}}=m_L+m_S$).

System	H_{appl} (T)	r (eV)	n_h	$p\times10^2$ (eV)	$q\times10^2$ (eV)	m_L/m_S	$m_L\times10^3$ (μ_B/Pt)	$m_S\times10^3$ (μ_B/Pt)	$m_{\mathrm{at}}\times10^3$ (μ_B/Pt)
Pt_{13}	6	8.30	1.85(2)	−5.05(4)	−3.72(7)	0.32(2)	5.49(9)	17.1(6)	22.6(9)
$Pt_{13}H_m$	6	8.53	1.87(2)	−6.22(6)	−4.37(9)	0.29(2)	6.39(7)	21.8(6)	28.2(9)
Pt foil	7	7.44	1.73(3)	−1.69(4)	−1.35(4)	0.38(2)	2.1(1)	5.5(1)	7.6(1)

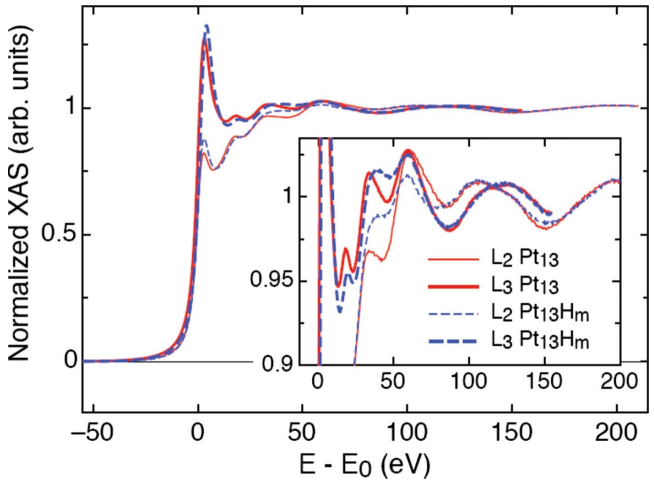

FIG. 7. (Color online) XAS Pt $L_{2,3}$-edges spectra of the Pt_{13} desorbed and $Pt_{13}H_m$, normalized to a common limit at the continuum. Inset: expanded view of the oscillations in the XANES region

The L_3 edge gives information on the empty valence-band levels (ΔVB) of both the $d_{5/2}$ and $d_{3/2}$ bands, weighted as $d_{5/2}/d_{3/2}=6$ (Ref. 15). On the other hand the L_2 reflects only the $d_{3/2}$ level. In Pt_{13}, as in small Pt clusters, the $5d_{3/2}$ is considered to be completely filled so the ΔVB may just be related to the $5d_{5/2}$ band, therefore, the difference yields ΔVB [L_3(Pt)-L_2(Pt)=ΔVB], which is shown in Fig. 8(a).

In Ref. 14 it is argued that the difference between the L_3 absorption edges of the bare and H-adsorbed clusters is due to two contributions: the electronic one due to the antibonding empty states (AS), and the change in the geometrical contribution to atomic x-ray absorption fine structure (ΔXAFS) caused by any additional Pt-H scattering and changes in the Pt-Pt distances, i.e., [L_3(Pt/H)-L_3(Pt) =ΔXAFS+AS]. On the other hand, the L_2 edges do not contain any valence-band contribution, therefore, the difference between the $Pt_{13}H_m$ and Pt_{13} is only due to ΔXAFS, i.e., [L_2(Pt/H)-L_2(Pt)=ΔXAFS]. The result of ΔXAFS is shown in Fig. 8(b), and peaks at 4.5 eV. From comparison to calculated values with FEFF8 code of Pt-H clusters,[19] we may conclude that the average Pt-H distance is slightly larger than that found for weakly bonded hydrogen on Pt/K-Al_2O_3 zeolite (R=1.95 Å).

From the difference of the ΔXAFS+AS and ΔXAFS one obtains the AS contribution [see Fig. 8(c)]. It amounts to a Fano resonance due to the existence of an antibonding state degenerate with a continuum state. The resonance data was fitted to the expression

$$\chi(\varepsilon) = A \sin \phi(1 - \varepsilon \cdot \cot\varepsilon)/(1 + \varepsilon^2), \qquad (1)$$

where $\varepsilon=(E-E_{res})/\Gamma$, φ is the EXAFS phase, E_{res} is the resonance energy, and Γ is the resonance width [Fig. 8(c)]. The positive value of E_{res}=2.3(1) eV is quite different to most examples of H adsorbed by Pt clusters described in the literature,[14,19,20] except for H-Pt on LTL(0.63) zeolite (E_{res} =2.1 eV).[14] It was argued that a positive E_{res} could be related to acidic character of the support or also reflect a less

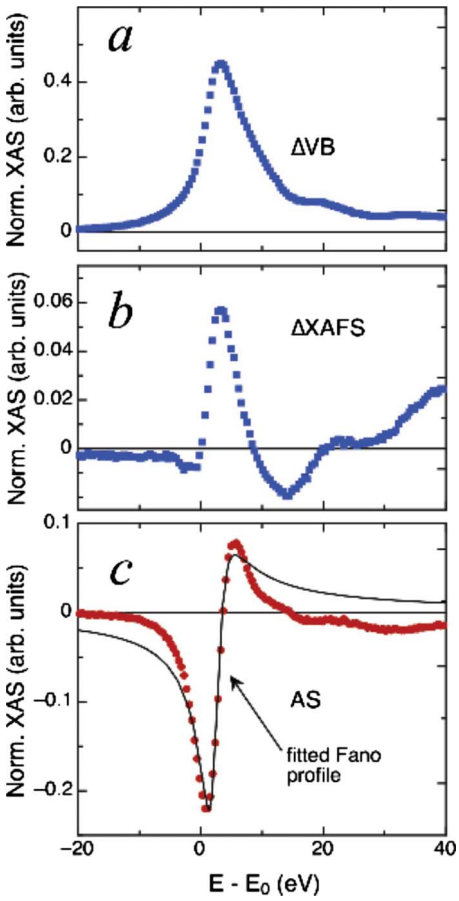

FIG. 8. (Color online) (a) ΔVB, $5d_{5/2}$ empty valence-band states. (b) ΔXAFS, due to Pt-H scattering. (c) Shape resonance of the Pt-H antibonding state for the adsorbed Hydrogen in $Pt_{13}H_m$. (—) Fit to Fano-resonance profile.

metallic character due to its small particle size.[14] In the Pt_{13} case it is probably due to the second effect given the nearly closed-shell character of the particle. The natural width of the resonance Γ is related to the quantum-mechanical matrix element, V, involving the Pt valence band and the Pt-H AS ($\Gamma=2\pi V$). The value obtained (Γ=1.8 eV) is comparable to that found in H-Pt/LTL(0.63) (Γ=2.1 eV), indicating a similar V interaction. The background phase parameter is positive (φ=0.58 rad) and close to that of H-Pt/LTL(0.63) (φ =0.47 rad). All these features indicate that the Pt-H antibonding state exists and is above the Fermi energy, in spite of core-hole attraction. As conclusion, we have proven that a part of the increase in n_h due to hydrogenation originates in the appearance of an antibonding state above the $5d_{5/2}$ band and above the Fermi energy.[19]

IV. XMCD RESULTS

The experiments on the Pt foil and cluster samples were performed at T=7 K and a field of H=6 T. The experimental XMCD data are of excellent signal-to-noise ratio [Figs. 2(b), 3(b), and 4(b)].The XMCD technique at the $L_{2,3}$ edges of Pt probes the empty $5d$ localized or band states above the Fermi energy, thus providing information on the averaged

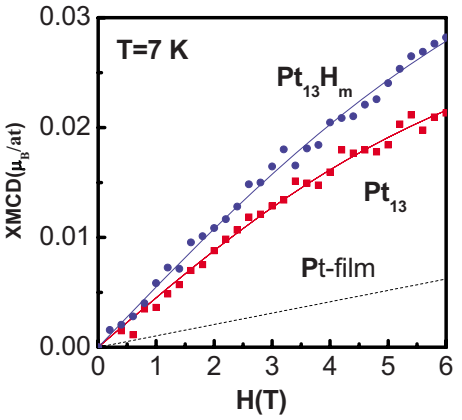

FIG. 9. (Color online) XMCD(H) curves for (■) Pt_{13} desorbed and (●) $Pt_{13}H_m$. Fits of the XMCD(H) data of Pt_{13} to Eq. (2). for (—) Pt_{13}, (—) $Pt_{13}H_m$. (···) Extrapolation for Pauli paramagnetic bulk Pt magnetization polarized by the applied field, as deduced from the XMCD data.

magnetic moments (in μ_B/Pt) caused by the filled states. One obtains, through the sum rules,[21,22] the spin and orbital moments averaged over the core and the surface of the particle. The sum rules have been applied to the spectra to derive the orbital, spin, and total magnetic moments, and the symbols and sign criteria defined in Ref.23 have been used below. The constant $C=(I_{L2}+I_{L3})/n_h$, as well as n_h, have been deduced in the previous section. It is noteworthy that in the present case of particles, with their anisotropy axes oriented at random, the dipolar term m_D cancels out so that the sum rule $(A-2B)=-Cm_S/\mu_B$ yields the spin component m_S (Ref. 10), A and B are the integrated areas of the L_3 and L_2 XMCD peaks, respectively. In Figs. 2(b), 3(b), and 4(b), the parameters $p=A$ and $q=A+B$ have been depicted. The results are included in Table I.

Field-dependent XMCD at the maximum of the L_3 peak was performed between +6 and −6 T, and vice versa. This process was done several times (six on average) and the signal was averaged over all the measurements and folded as to average the first and third quadrants of the M vs H plot, i.e., the absolute values of the M and H points were considered. This was done to increase the signal-to-noise ratio. Moreover, the absolute scale, in μ_B/Pt, was fixed at $H=6$ T to the values of $m_{at}=m_L+m_S$ derived above from the sum rules. The resulting XMCD(H) data are plotted in Fig. 9.

The XMCD experiment is element selective, therefore it is guaranteed that the XMCD signal is caused exclusively by the Pt contained in the sample. Magnetic impurities other than Pt, such as Fe at the ppm level, as mentioned to be present in the zeolite,[8] do not give any contribution.

The mean magnetic moment per Pt ($m_{at}=22.6\times10^{-3}$ and 28.2×10^{-3} μ_B/Pt for Pt_{13} and $Pt_{13}H_m$, respectively) is much larger than the experimental values reported for the field-induced moment by Pauli paramagnetism (PP) in Pt metal for the same applied field ($H=6$ T). Indeed, from XMCD at the $L_{2,3}$ edges on a Pt thin film the value $m_{at}=7.6\times10^{-3}$ μ_B/Pt, at $T=10$ K and $H=7$ T has been determined (see Table I). The linear field dependence of Pt as a Pauli paramagnet is shown for comparison in Fig. 9. As conclusion, we can disregard a field-induced moment by PP as the source of the magnetic signal we observe by XMCD. Besides, the XMCD(H) experimental data show a negative curvature, more remarkable for the Pt_{13} desorbed sample, which is incompatible with a PP field-induced magnetism.

V. DISCUSSION

To understand the m_L, m_S, and m_L/m_S results obtained above it is necessary to compare them with those for magnetic Pt in other configurations. For this purpose the available data have been collected in Table II. As said above, the quality of the XMCD data is excellent, thus, the values found are reliable from the experimental point of view, $m_S=17.1\times10^{-3}$ μ_B, $m_L=5.5\times10^{-3}$, and $m_L/m_S=0.32$ for Pt_{13}.

If these values are compared to the Pauli paramagnetic Pt (Pt-foil entry in Table II), it is obvious that at the maximum field $H=6$ T the m_S and m_L values for Pt_{13} and $Pt_{13}H_m$ are about four times larger per Pt atom. However, in the Pt foil the ratio $m_L/m_S=0.38$ is larger than in the Pt_{13} clusters.

The ratio $m_L/m_S=0.32$ found for the Pt clusters is larger than the values found in other magnetic Pt systems different than the Pt foil. However, our data of m_L, m_S, and m_T, with little difference between the Pt_{13} and the $Pt_{13}H_m$, are one order of magnitude smaller than the observed ones in samples where the magnetism has been induced by hybridization with magnetic metals (see Table II). To understand this difference the field-dependent XMCD data need to be analyzed.

Magnetically, the Pt_{13}-NaY system behaves as a superparamagnetic uncoupled cluster. The only possible magnetic interaction would be the long-range dipolar one, given the sparse distribution of clusters in the lattice. Indeed, we observe no hint of interaction either in the absence of a Curie-Weiss temperature in the fit of the high-temperature susceptibility[9] or in the EPR spectra.[8] To be sure of this approximation, we have performed an estimation of the mean field of dipolar origin in the worst case, i.e., assuming that all moments were aligned in the same direction. The calculation of the dipolar energy on a probe cluster of 3.7 μ_B was done by Monte Carlo simulation of a random distribution of identical clusters in the cubic NaY zeolite, using the distances and Pt_{13} charge given in the introduction, i.e., one Pt_{13} cluster every 25 and just 20% of them being magnetic (see below). The dipolar energy converges to the value of $E_{dip}/k_B=63$ mK, which is negligible compared with the thermal energy at 7 K, the experimental temperature. So, the approximation of uncoupled magnetic clusters is well justified.

The field dependence of the magnetization is well described by the classical Langevin function μ being the average magnetic moment per particle and f the fraction of magnetic atoms per mol, when M is given in units of emu/mol

$$M(H)=fN_A\frac{\mu}{13}\left[\coth\left(\frac{\mu H}{k_BT}\right)-\frac{k_BT}{\mu H}\right]+\chi_0 H. \qquad (2)$$

χ_0 is assumed to be a temperature-independent susceptibility due to possible Pt in Pauli paramagnetic state, errors in the substrate subtraction, or others. The prefactor in the first term

TABLE II. Comparison of m_L, m_S, and m_L/m_S of the 5*d* states of Pt, obtained from XMCD at the L_2 and L_3 edges. H_{app}, the applied field at which the measurement was performed.

System	H_{appl} (T)	m_L/m_S	$m_L\times10^3$ (μ_B/Pt)	$m_S\times10^3$ (μ_B/Pt)	$m_{at}\times10^3$ (μ_B/Pt)
Pt_{13} desorbed	6	0.32(2)	5.49(9)	17.1(6)	22.6(9)
$Pt_{13}H_m$	6	0.29(2)	6.39(7)	21.8(6)	28.2(9)
Pt foil	7	0.38	2.1	5.5	7.6
Pt/Co bilayer[a]	5				180
Pt/Co bilayer [b]					210
Pt/Co interface[c]	2	0.16	53	333	386
Pt_3/Co_{13} Interface[d]	5	0.23	128	550	680
$Pt_{50}Co_{50}$ Nanopart[e]	0.6	0.30	70.1	230	300
$Pt_{50}Fe_{50}$ Nanopart[f]	2.8	0.13	54	410	464
$Pt_{50}Co_{50}$ Thin film[g]	5	0.27	90	350	440
$CoPt_3$ Thin film[h]	4	0.26	58	220	278

[a]Reference 24.
[b]Reference 1.
[c]Reference 2.
[d]Reference 26.
[e]Reference 5.
[f]Reference 4.
[g]Reference 25.
[h]Reference 16.

of Eq. (2) scales the Langevin curve, giving information on the total magnetic moment in the sample and therefore on the number of atoms giving rise to that magnetization while from the shape of the Langevin curve the information on the magnetic moment of the individual particle μ is deduced. This curvature does not depend on the total magnetization. The parameter $f=13N/N_A$ informs of the fraction of the total number of Pt atoms per mol that are magnetic. Therefore, one obtains two independent pieces of information, the magnetic moment of the particle μ and the fraction f.

From the fit to the data in Fig. 9 one obtains for the Pt_{13} cluster the average value of $\mu=3.7\pm0.4$ μ_B and $f=0.14\pm0.1$, that is, about 15% of the Pt contribute to the magnetic XMCD signal. For the $Pt_{13}H_m$ the curvature is smaller than for Pt_{13} and the fit yields values of $\mu=3.0\pm0.4$ μ_B and $f=0.2\pm0.1$. The temperature-independent paramagnetic term is considered negligible, as derived from magnetic measurements.[9] In the case of $Pt_{13}H_m$ $\mu=3.0\pm0.4$ μ_B and the fraction of magnetic Pt_{13} about 10–20%. Since it cannot be excluded that the sample in our experiment could be at a slightly higher temperature than that at the thermometer in contact with the capsule because the unavoidable zeolite bad thermal-conduction properties, the actual μ values could be somewhat higher, but never smaller, than the values we report above (an increase to $T=8$ K would imply that $\mu=4.2$ μ_B in Pt_{13}). These results may be compared with the magnetic moment ($m_{Pt}=0.45$ and 0.43 μ_B, for Pt_{13} and $Pt_{13}H_m$, respectively) extracted from the $M(H)$ SQUID measurements at $T=1.8$ K on the same type of samples.[9] The corresponding average particle moments are $\mu=5.9\pm0.1$ and 5.6 ± 0.1 μ_B, and the magnetic fraction of Pt participating in the formation of magnetic clusters are $f=0.14\pm0.01$ and 0.10 ± 0.01, for Pt_{13} and $Pt_{13}H_m$, respectively.

In both sets of data, XMCD and SQUID, the cluster moment of the Pt_{13} cluster is larger than that of the $Pt_{13}H_m$ one. On the other hand, the magnetic-moment absolute values from XMCD are of the same order of magnitude but smaller than those derived from the SQUID measurements while the fraction f of magnetic Pt is similar, within the error. The low fraction $f\approx0.1$–0.2 of magnetic Pt may explain the very low EPR signal ($\approx0.03\%$) which could be detected in the $Pt_{13}H_m$ and $Pt_{13}D_m$ samples.[8] Besides, the EXAFS and XAS analysis indicate that the samples consist mainly of Pt_{13} reduced or desorbed Pt_{13} clusters, respectively. Both observations and the low value of f imply that a fraction (1-f) of Pt is actually forming nonmagnetic Pt_{13} clusters, i.e., clusters with a ground state $S=0$.

The reason to have such a large fraction of nonmagnetic cluster, both in the bare and the hydrogenated cases, remains unclear. There are, definitely, some water molecules as by-product of the reduction process with H since the temperature in this process cannot be too high. The combination of oxygen and water vapor are known to quench the EPR signal after long exposure, but we have been extremely careful during the preparation and sample handling of assuring absence of oxygen, so we do not think this is the reason for the large number of nonmagnetic clusters. Besides, interaction with the zeolite may take place via the residual Na^+ ions, which are randomly distributed, since only one out of close to four, on average in a supercage, are exchanged. Other possible interactions may occur with the Brønsted acid protons remaining after the reduction in Pt^{2+} to Pt^0 in the ion exchange first stage of the preparation process, which are located at the

O atoms near the Al atoms. Therefore, not all of the clusters see the same environment and there could be a modification of the electronic ground state of the cluster because of charge exchange with some of these ions or protons.

At this stage it is pertinent to revise the validity of the determination of the n_h for Pt_{13} clusters, presented in Sec. III. The value found (Table I) corresponds to the average over all clusters, magnetic and nonmagnetic, thus if each of these two species has a different n_h the values of m_L and m_S found for Pt_{13} cluster may be different. However, the average n_h is calculated from the area difference with respect to the absorption XANES of Au and differ from that of Pt foil by 5%. So a lower limit for the Pt_{13} cluster n_h may be considered as that of the Pt foil, assuming that the nonmagnetic species are those in which holes are created, in which case the values of m_L and m_S would be 5% smaller than given in Table I. The upper limit is found under the assumption that the increase in n_h would correspond just to the magnetic species, then the m_L and m_S could deviate at most by 30%. Therefore, the absolute values of the magnetic moments given in Table I should be regarded as valid within those thresholds. On the other hand, the ratio m_L/m_S does not depend on the value of n_h so the value given in Table I $[m_L/m_S=0.32(2)]$ is very reliable and indicates that the orbital component m_L plays an important role in the magnetic properties of the Pt_{13} magnetic species.

The very small increase in n_h of $Pt_{13}H_m$ with respect to the Pt_{13} cluster corresponds to the difference in XANES areas between them. Since the relative amount of magnetic and nonmagnetic species is similar, the relative variation in m_L and m_S caused by hydrogen uptake, and the analysis given in Sec. III are devoid of this shortcoming in the determination of n_h.

At any rate and under this note of attention to the possible deviations of m_L and m_S from the average values, we analyze below the implications on the electronic structure of the magnetic clusters. In this work we conclude that the Pt_{13} cluster-moment value lays in the range $\mu \approx 3.5-4.9\ \mu_B$ On the other hand, from the $M(H)$ SQUID measurements the value $\mu \approx 5.9\ \mu_B$ was found.[9] So, there is, admittedly, a large uncertainty on the actual value. Under the simple assumption currently done that the cluster magnetic moment has its origin in the unpaired number of electrons the ground state of the studied system lays in the range of total spin $S=2-3$.

This result may be compared to some theoretical predictions. In Ref. 27 the energy levels, density of states, and total energy of cuboctahedral and icosahedral free Pt_{13} clusters were calculated, including spin-orbit coupling and Jahn-Teller (J.T.) distortion in the energy optimization calculations to find the most stable configuration. It was found for a cluster spin $S=3$ in cuboctahedral symmetry, distorted by J.T. effect to D_{4h} symmetry. Close in energy, but less stable, is the configuration with $S=4$ and icosahedral symmetry, distorted by J.T. to C_{2h} symmetry. Besides, in different DFT calculations of the electronic cluster energy, the ground-state cluster spin of icosahedral Pt_{13} and $Pt_{13}H_n$ clusters were predicted.[8] They show that the magnetic state of a cluster depends strongly on the hydrogen coverage and on the cluster charge. In this calculation the value found was $S=1\ \mu_B$ with distorted icosahedral symmetry, which is far too low with respect to the experimental result. If the cluster is not neutral or has undergone incomplete desorption with one H atom adsorbed, i.e., Pt_{13}^+ or $Pt_{13}H^+$ the calculation yields in the former case $S=3/2$ while in the latter $S=1$, 3/2 or 2, depending on the site location of the H atom on the cluster surface. In both cases, the predicted moments are closer to our experimental result. However, neither of the two sets of calculations has tried to obtain the separate orbital and spin contributions to the magnetic moment, or else, calculate total angular momentum as origin of the magnetic moment so we cannot compare our results on orbital magnetic moment with any theoretical ones.

In spite of the discrepancies with the experimental results, the calculations show that the ground state may be a high nonzero spin state, as found. The above model systems consider a free Pt_{13} cluster; i.e., does not take into account any interaction with the support but seem to reflect the essential physics of the cluster system.

Let us address the question whether the 13 Pt atoms participate equally or just the 12 surface ones are the magnetogenic atoms. From the mentioned EPR results, where the multiplets were fitted with a simulation considering only 12 magnetic Pt per cluster, one concludes that only the 12 peripheral Pt contribute magnetically. Therefore, the average total moment per surface Pt is in the range $m_{Pt} \approx 0.3-0.4\ \mu_B$ and from $m_L/m_S=0.32$, an orbital moment of $m_L \approx 0.1-0.13\ \mu_B$ and spin moment $m_S \approx 0.20-0.30\ \mu_B$ are deduced. While m_S is comparable to the values found in other Pt containing systems, m_L is larger than any previous determination on magnetic Pt by hybridization with transition metals. The large m_L may be related to the fact that in surface atoms, the orbital moment perpendicular to the cluster surface tends to increase. Such an effect has been observed earlier in Co particles embedded in alumina or capped with Cu, Ag, and Au.[28–30] It was explained as due to the Co $3d$ electron surface quasiband states narrowing due to the breaking of symmetry at the Co vacuum or Co/metal interface. This conjecture is based on the similarity of the surface d states calculated for a Pt_{13} cluster (cuboctahedron) which are analogous to the surface states of crystalline transition metals.[31]

VI. CONCLUSIONS

The XAS results offer us some important information. The agreement of the L_3-edge spectra to the calculated XAS for a Pt_{13} cluster[13] explains the geometrical and electronic modifications in the low-energy EXAFS region with respect to the Pt foil and reassures us of the majority presence of Pt_{13} clusters in the loaded NaY zeolite. The comparison to the $L_{2,3}$ edges of Au permits the determination of the available average number of holes $n_h=1.85$ and 1.87, for Pt_{13} and $Pt_{13}H_m$ above the Fermi energy, i.e., the ΔVB contribution to the spectra in Pt_{13} and the ΔVB and AS in $Pt_{13}H_m$. The analysis of the differences in the $L_{2,3}$ edges between the Pt_{13} and $Pt_{13}H_m$ samples shows the presence of a Fano resonance caused by the Pt-H antibonding state, with $E_{res}=2.3$ eV. The strength of the bond is deemed to be weak, thereby propos-

ing that H is chemisorbed by the Pt cluster.[20]

The XMCD measurements show without ambiguity that the Pt_{13} cluster supports a magnetic moment. The XMCD(H) field dependence can be explained as due to the superparamagnetic behavior of the localized cluster moment μ. It is also shown that the magnetic behavior is incompatible with Pauli paramagnetism, therefore, the cluster has no metallic character. Indeed, molecular-orbital calculations lets describe the electronic states of the cluster in terms of MO s and p shells and atomic d states.[27] On the other hand, the density of states near the Fermi surface resembles that of Pt metal.[30] It seems that in the Pt_{13} clusters the discreteness of the electronic states due to small size effect and therefore, also due to the predominancy of the surface effect, deviates the system from metallic behavior. For a Pt_{13} cluster the magnetic moment obtained is $\mu \approx 3.5-4.9\ \mu_B$, with 32% originating from the orbital momentum. The moment of the $Pt_{13}H_m$ is somewhat lower, $\mu \approx 3.-4.\ \mu_B$. Only a small fraction, $f \approx 15-20\%$, of the Pt atoms, forming Pt_{13} or $Pt_{13}H_m$ clusters, contribute to the Pt XMCD signal.

The EPR, on one hand, and the SQUID and XMCD data, on the other hand, show that only a small fraction of all the Pt clusters contribute to the magnetic response, even in the case of desorbed Pt_{13}. This fact remains unsolved, though one may conjecture that the NaY zeolite may exchange charge with the Pt_{13} cluster, thus making the cluster magnetically silent. The Pt_{13} cluster spin lays in the range $S \approx 2-3$ as deduced from our XMCD analysis and from SQUID measurements. At any rate, both experimental results are much larger than the DFT calculated spin $S=1$ ground state for a free icosahedral cluster but are closer to the predicted values for Pt_{13}^+ or the incompletely desorbed $Pt_{13}H^+$ clusters.[8] When comparing to theoretical predictions a note of caution should be given; it seems that the approximation of the zeolite playing no role in the magnetic properties of the Pt_{13} clusters is too strong, therefore, the Pt_{13}-zeolite interaction should be taken into account.

Besides, though the calculations of the Pt electron bands have taken into account spin-orbit effects, there are, so far, no predictions for the orbital momentum of a Pt_{13} cluster. Our result unambiguously proves that $m_L/m_S=0.32$, that is, a very important fraction of the magnetic moment is supplied by the orbital momentum and by comparison to the lower values of the m_L/m_S ratio found in Co/Pt films, for example, we ascribe this effect to a larger contribution to orbital moment by the predominant surface Pt atoms in the Pt_{13} clusters, which have a very different Pt near-neighbor surrounding than in the bulk or in a Pt thin film. The electronic-structure calculations available to date indicate the existence of surface states,[27,30] similar to surface bands in films, that may support an enhanced orbital momentum or anisotropy. We expect that this result will encourage further theoretical work on the magnetism of Pt clusters.

ACKNOWLEDGMENTS

This work has been partly funded by Grants No. MAT08-1077 and No. MAT05-02454 from MICIN, and PM-012, IMANA, and CAMRADS from DGA. Y.A. thanks the Deutsche Forschungsgemeinschaft for financial support through the Research Training Group GK448. Fruitful discussions with J. Chaboy are acknowledged.

[1] J. Geissler, E. Goering, M. Justen, F. Weigand, G. Schütz, J. Langer, D. Schmitz, H. Maletta, and R. Mattheis, Phys. Rev. B. **65**, 020405(R) (2001).
[2] M. Suzuki, H. Muraoka, Y. Inaba, H. Miyagawa, N. Kawamura, T. Shimatsu, H. Maruyama, N. Ishimatsu, Y. Isohama, and Y. Sonobe, Phys. Rev. B **72**, 054430 (2005).
[3] J. Bartolomé, L. M. García, F. Bartolomé, F. Luis, F. Petroff, C. Deranlot, F. Wilhelm, and A. Rogalev, J. Magn. Magn. Mater. **316**, e9 (2007).
[4] C. Antoniak, J. Lindner, M. Spasova, D. Sudfeld, M. Acet, M. Farle, K. Fauth, U. Wiedwald, H.-G. Boyen, P. Ziemann, F. Wilhelm, A. Rogalev, and S. Sun, Phys. Rev. Lett. **97**, 117201 (2006).
[5] N. Jaouen, D. Babonneau, J. M. Tonnerre, D. Carbone, F. Wilhelm, A. Rogalev, T. K. Johal, and G. van der Laan, Phys. Rev. B **76**, 104421 (2007).
[6] Y. Yamamoto, T. Miura, Y. Nakae, T. Teranishi, M. Miyake, and H. Hori, Physica B **329-333**, 1183 (2003).
[7] Y. Akdogan, Ch. Vogt, M. Bauer, H. Bertagnolli, L. Giorgiu, and E. Roduner, Phys. Chem. Chem. Phys. **10**, 2952 (2008).
[8] X. Liu, H. Dilger, R. A. Eichel, J. Kunstmann, and E. Roduner, J. Phys. Chem. B **110**, 2013 (2006).
[9] X. Liu, M. Bauer, H. Bertagnolli, E. Roduner, J. van Slageren, and F. Phillipp, Phys. Rev. Lett. **97**, 253401 (2006); **102**, 049902(E) (2009).
[10] Y. Akdogan, S. Anantharaman, X. Liu, G. K. Lahiri, H. Bertagnolli, and E. Roduner, J. Phys. Chem. C **113**, 2352 (2009).
[11] J. Stöhr, J. Magn. Magn. Mater. **200**, 470 (1999).
[12] O. Hjortstam, J. Trygg, J. M. Wills, B. Johansson, and O. Eriksson, Phys. Rev. B **53**, 9204 (1996).
[13] A. L. Ankudinov, J. J. Rehr, J. J. Low, and S. R. Bare, J. Chem. Phys. **116**, 1911 (2002).
[14] D. E. Ramaker, B. L. Mojet, M. T. Garriga Oostenbrinck, J. T. Miller, and D. C. Koningsberger, Phys. Chem. Chem. Phys. **1**, 2293 (1999).
[15] L. F. Mattheiss and R. E. Dietz, Phys. Rev. B **22**, 1663 (1980).
[16] W. Grange, M. Maret, J.-P. Kappler, J. Vogel, A. Fontaine, F. Petroff, G. Krill, A. Rogalev, J. Goulon, M. Finazzi, and N. B. Brookes, Phys. Rev. B **58**, 6298 (1998).
[17] I. Galanakis, M. Alouani, and H. Dreyssé, J. Magn. Magn. Mater. **242-245**, 27 (2002).
[18] B. Hammer and J. K. Nørskov, Nature (London) **376**, 238 (1995).
[19] D. C. Koningsberger, M. K. Oudenhuijzen, J. H. Bitter, and D. E. Ramaker, Top. Catal. **10**, 167 (2000).
[20] M. K. Oudenhuijzen, J. H. Bitter, and D. C. Koningsberger, J. Phys. Chem. B **105**, 4616 (2001).
[21] P. Carra, B. T. Thole, M. Altarelli, and X. Wang, Phys. Rev. Lett.

70, 694 (1993).
[22] B. T. Thole, P. Carra, F. Sette, and G. van der Laan, Phys. Rev. Lett. **68**, 1943 (1992).
[23] J. Stöhr, J. Electron Spectrosc. Relat. Phenom. **75**, 253 (1995).
[24] P. Poulopoulos, M. Angelakeris, E. Th. Papaioannou, N. K. Flevaris, D. Niarchos, M. Nyvlt, V. Prosser, S. Vinovsky, Ch. Mueller, P. Fumagalli, F. Wilhelm, and A. Rogalev, J. Appl. Phys. **94**, 7662 (2003).
[25] W. Grange, I. Galanakis, M. Alouani, M. Maret, J.-P. Kappler, and A. Rogalev, Phys. Rev. B **62**, 1157 (2000).
[26] F. Wilhelm, P. Poulopoulos, A. Scherz, H. Wende, K. Baberschke, M. Angelakeris, N. K. Flevaris, J. Goulon, and A. Rogalev, Phys. Status Solidi A **196**, 33 (2003).
[27] N. Watari and Sh. Ohnishi, Phys. Rev. B **58**, 1665 (1998).
[28] F. Luis, F. Bartolomé, F. Petroff, J. Bartolomé, L. M. García, C. Deranlot, H. Jaffrès, M. J. Martísnez, P. Bencok, F. Wilhelm, A. Rogalev, and N. B. Brookes, Europhys. Lett. **76**, 142 (2006).
[29] J. Bartolomé, L. M. García, F. Bartolomé, F. Luis, R. López-Ruiz, F. Petroff, C. Deranlot, F. Wilhelm, A. Rogalev, P. Bencok, N. B. Brookes, L. Ruiz, and J. M. Gonzalez-Calbet, Phys. Rev. B **77**, 184420 (2008).
[30] L. M. García, F. Bartolomé, J. Bartolomé, F. Luis, F. Petroff, C. Deranlot, F. Wilhelm, A. Rogalev, P. Bencok, and N. Brookes, J. Magn. Magn. Mater. **316**, e23 (2007).
[31] R. P. Messmer, S. K. Knudson, K. H. Johnson, J. B. Diamond, and C. Y. Yang, Phys. Rev. B **13**, 1396 (1976).